Investigation into Etching Mechanism of Polyethylene Terephthalate (PET) Films Treated in Helium and Oxygenated-Helium Atmospheric Plasmas

Suzanne R. Matthews,[1] Yoon J. Hwang,[1] Marian G. McCord,[1] Mohamed A. Bourham[2]

[1]*North Carolina State University, Department of Textile Chemistry, Engineering, and Science, Raleigh, North Carolina*
[2]*North Carolina State University, Department of Nuclear Engineering, Raleigh, North Carolina*

Received 19 December, 2003; accepted 4 April, 2004
DOI 10.1002/app.21162
Published online 22 October 2004 in Wiley InterScience (www.interscience.wiley.com).

ABSTRACT: This research makes an investigation into the etching mechanism of atmospheric plasma conditions on the surface of polyethylene terephthalate (PET) films. Two types of untreated PET films (S/200 and S/500) were exposed to plasma for 0 to 5.0 min in 30-s increments. The first set of each film type was treated in helium plasma, while the second was treated in oxygenated-helium plasma. Differential Scanning Calorimetry (DSC) was used to characterize pre- and post-exposure films. Weight changes and the degree of solubility were also determined. Based on peak area results, the percent crystallinity of PET S/200 increased by an average of 4.57% (helium treated) and 13.56% (oxygenated-helium treated), while the S/500 showed only a small increase. There was no significant change in the melting or crystallization temperatures of either film type, indicating a decrease in amorphous content versus an increase in crystalline material. Weight loss analysis supports this theory. Solubility testing revealed a continual decrease in swelling as exposure time was increased. A model was developed to predict the change in the degree of solubility for polyphase surfaces considering the etching rate per phase. The model was applied to PET with good correlation between the model and experimental data. © 2004 Wiley Periodicals, Inc. J Appl Polym Sci 94: 2383–2389, 2004

Key words: films; surfaces; modifications; modeling; plasma

INTRODUCTION

Surface modification of textile materials, such as films, fabrics, and nonwovens, has always been a highly focused area of research. By altering the physical and chemical characteristics of a given material, new products and applications can be created. These processes, however, can involve numerous chemicals, some of which are toxic to humans and hazardous to the environment. Out of this concern come new alternatives to surface modification, one of the most recent being plasma treatment. This procedure not only eliminates the need for wet processing, but it also yields unique surface characteristics. Several modifications include, but are not limited to: hydrophilicity/hydrophobicity alterations, surface roughening, grafting, and surface functionality.[1–10] While these novel changes are possible, only vacuum treatments have been thoroughly analyzed and documented. An ideal process would include an atmospheric plasma chamber to allow for continuous processing; however, modeling and mechanisms in atmospheric pressure plasma have not been thoroughly investigated. The aim of this study is to investigate the mechanism of surface interactions and to develop a model for the effects of atmospheric pressure plasma on polyethylene terephthalate (PET) films, specifically the change in surface etching and solubility. Investigation of these films will be further extended into the studies of PET polymers in fabric and fiber forms.

Two types of PET films (S/200 and S/500) with different thickness were exposed to plasma for 0 to 5.0 min in 30-s increments. The first set of each film type was treated in helium plasma, while the second was treated in oxygenated-helium plasma (99% helium/1% oxygen mix). Differential Scanning Calorimetry (DSC) was used to characterize pre- and post-exposure films. Weight changes and the degree of solubility were also determined.

EXPERIMENTAL

The atmospheric plasma facility

The atmospheric plasma facility has an active exposure area of approximately 60 × 60 cm between two copper electrodes with 5 cm gap separation. Each copper electrode is embedded in a polycarbonate dielectric barrier. The device is powered by a 4.8 kW power supply operating in the frequency range between 5 kHz and 10 kHz. The device has an inner

Correspondence to: S. R. Matthews (srmatthews01@hotmail.com).

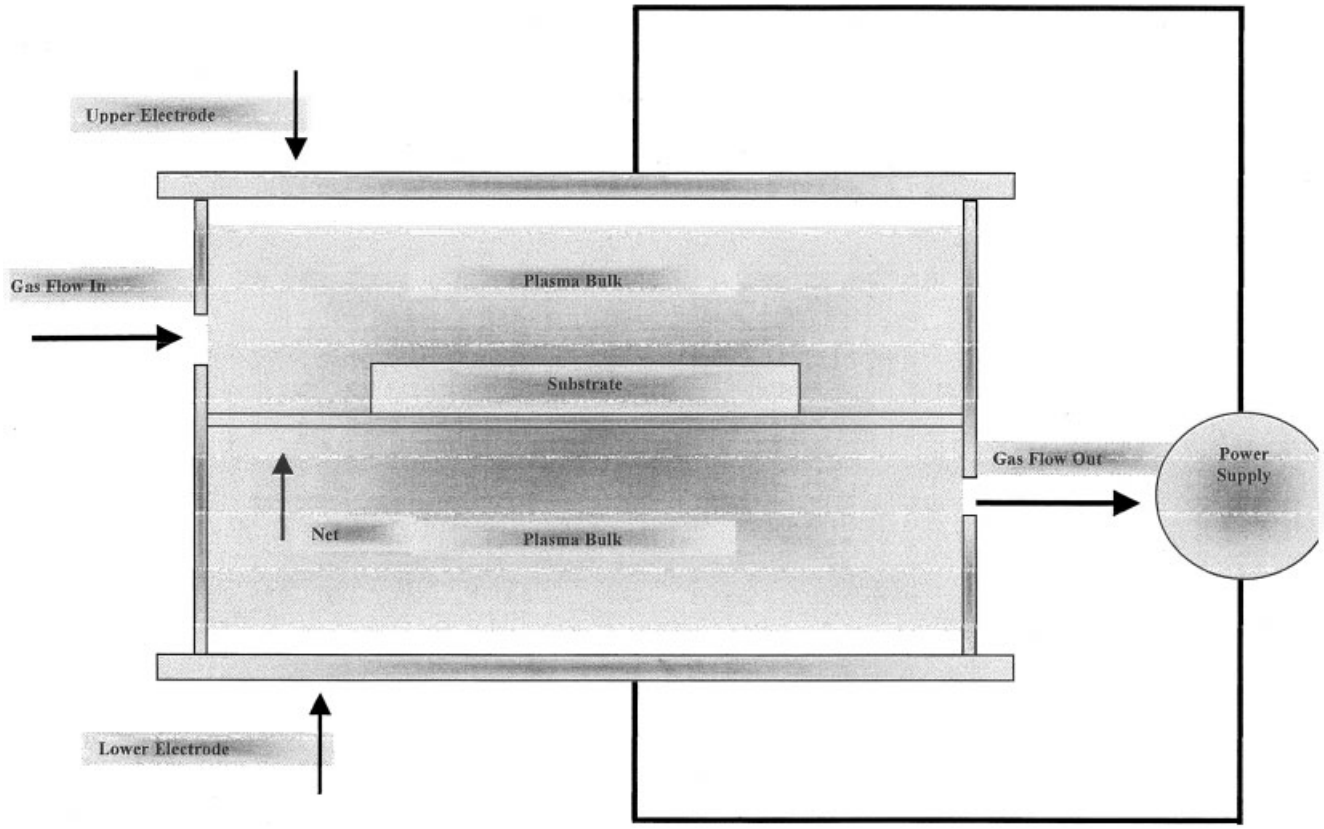

Figure 1 Schematic of the NCSU atmospheric plasma device.

plasma chamber installed inside of an outer chamber, where the latter is equipped with a fabric rolling system for continuous fabric modification treatments. The working gas is fed into the chamber through gas flow controllers. Figure 1 shows a schematic drawing of the experimental facility. When flowing helium or oxygenated-helium into the plasma chamber, there will always be a slight amount of air due to the fact that the chamber is not pumped down and operates at atmospheric pressure. The device is capable of batch treatment of films and fabric pieces using a test cell, as well as continuous operation using the roller feed system for large fabric rolls or continuous filaments and yarns. The PET films in this study were exposed to helium and oxygenated-helium plasma using the test cell. The test cell is a closed geometry chamber, with little to no ventilation, in which volatiles are not continuously removed. Samples are placed on a suspended nylon grid within the test cell, which allows for complete exposure to plasma on both sides of the substrate. For these experiments the operating frequency of the power supply was kept constant at 5 kHz. The exposure time was varied between 0.5 and 5.0 min in 30-s intervals. Input power, operating voltage, and plate separation were all held constant. The helium gas flow rate was held at approximately 10 L/m, and an additional flow of 1% oxygen was added for the mixed gas regime experiments. The plasma discharge inside of the test cell is uniform and free from coronas, which allows for uniform treatment of the exposed samples.

Materials

Melinex® polyethylene terephthalate (PET) films were obtained from DuPont Teijin Films (Wilmington, DE). These films were untreated and classified as slightly hazy. Except for the difference in thickness, both films were identical in composition, with a thickness of 50μm for the S/200 samples and 125 μm for the S/500 samples.

Characterization and analysis

Differential scanning calorimetry

Thermal analysis of the samples was conducted using a Perkin–Elmer 7 Differential Scanning Calorimeter (DSC). Each sample was scanned at a rate of 20°C/min over the range of 25°–300°C. The onset melting and crystallization temperatures were obtained from the intercept of the baseline and the maximum tangent of the corresponding exothermic and endothermic peaks. Peak areas were also calculated to evaluate the changes in percent crystallinity.

TABLE I
DSC Results of PET S/200 Treated in He

Exposure time (min)	Melt onset (°C)	Peak area (mJ)
0.0	244.91	166.31
0.5	245.27	167.97
1.0	244.44	150.85
1.5	254.67	155.04
2.0	246.14	178.67
2.5	248.07	174.19
3.0	245.34	179.40
3.5	245.30	195.75
4.0	244.57	172.46
4.5	248.19	175.98
5.0	245.61	188.81
Treated ave.	246.76	173.91
% change	+0.76	+4.57%

TABLE III
DSC Results of PET S/500 Treated in He

Exposure time (min)	Melt onset (°C)	Peak area (mJ)
0.0	245.43	171.20
0.5	246.17	177.22
1.0	244.12	172.66
1.5	246.45	165.62
2.0	245.68	161.08
2.5	247.38	208.63
3.0	244.53	171.86
3.5	247.03	172.59
4.0	244.25	160.24
4.5	243.45	186.06
5.0	244.49	182.33
Treated ave.	245.36	175.83
% change	+0.76%	+2.70%

Weight loss

Each sample was weighed before and after plasma treatment using an Explorer® microbalance with an accuracy of ± 100 μg to determine weight changes, gain or loss. The percent weight loss is plotted versus the exposure time for both S/200 and S/500 samples.

Surface analysis

Atomic Force Microscopy (AFM) analysis was performed, at a satellite location in North Carolina State University's engineering department to determine surface roughness and re-deposition.

Solubility

Portions of each film sample were soaked for 20 h in 100% toluene. The samples were weighed before and after soaking using a Denver Instrument® M-220D microbalance with an accuracy of ± 10 μg. Their swelling ability/degree of solubility was determined from the calculated weight difference.

RESULTS AND DISCUSSION

Differential scanning calorimetry

Results of Differential Scanning Calorimetry (DSC) showed slight fluctuations in the melt and crystallization onset temperatures, with the average temperature values being no more than 2°C higher than the control, as shown in Tables I–IV. No conclusions could be drawn from these measurements since no significant difference was observed. Following these results, the crystallinity for each film was analyzed based on the formula[11]:

$$\% \text{ Crystallinity} = \text{peak area}/\Delta H_o^f$$

where ΔH_o^f is the standard heat of formation; and since it is a constant value, the crystallinity is solely depen-

TABLE II
DSC Results of PET S/200 Treated in He/O_2

Exposure time (min)	Melt onset (°C)	Peak area (mJ)
0.0	244.91	166.31
0.5	245.97	156.48
1.0	245.62	191.10
1.5	246.17	181.10
2.0	248.64	176.48
2.5	246.49	190.57
3.0	243.32	197.54
3.5	246.82	214.43
4.0	245.49	200.51
4.5	244.71	185.42
5.0	244.06	195.04
Treated ave.	245.73	188.87
% change	+0.33%	+13.56%

TABLE IV
DSC Results of PET S/500 Treated in He/O_2

Exposure time (min)	Melt onset (°C)	Peak area (mJ)
0.0	245.43	171.20
0.5	246.00	170.36
1.0	244.59	163.63
1.5	242.08	162.53
2.0	245.99	182.72
2.5	246.87	180.12
3.0	244.44	181.05
3.5	245.11	152.09
4.0	246.07	166.27
4.5	245.64	177.19
5.0	245.50	161.68
Treated ave.	245.23	169.77
% change	−0.08%	−0.84%

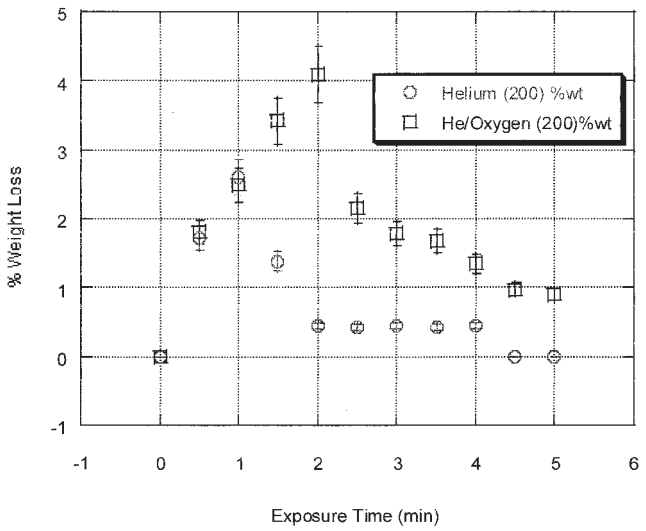

Figure 2 Percent weight loss versus exposure time for PET 200 treated in helium and oxygenated-helium plasmas.

dent on the endotherm peak area. Based on this calculation, there was a significant increase in % crystallinity noted for both the helium and oxygenated-helium exposed S/200 films. Specifically, there was a 4.57% average increase in the helium exposed films, and a 13.56% increase in the oxygenated-helium exposed films. This same increase was observed when analyzing the exotherm peak area. In contrast, the S/500 films exhibited little to no change in % crystallinity. This minimal effect is most likely due to the larger thickness of the S/500 films. With this increased bulk, the DSC may not be as sensitive to the surface treatment.

The notable increase in % crystallinity for the S/200 films may be explained by several possible mechanisms: (1) an elevation in temperature from plasma exposure creates thermal energy in the polymer chains, which then move to form new crystals or cause small crystals to grow in size; (2) etching creates spacing in the polymer network, allowing for chain movement and further crystallization; (3) amorphous regions are selectively etched due to ease of removal, thereby shifting the crystalline/amorphous ratio. As amorphous content is decreased, the percent crystallinity is automatically increased. Since no change was observed for the melt and crystallization onset temperatures, which would indicate an increase in crystalline content, the most probable mechanism is a decrease in the amorphous regions by selective etching. This mechanism was previously proposed by Okuno et al. when testing the dyeability of PET treated in a vacuum plasma.[12] The following sections will further develop the validity of this mechanism.

Weight loss

This experimental configuration allows for surface etching with an increased etching rate until reaching saturation inside of the test cell. As no ventilation is allowed, re-deposition of etched volatiles will be eminent. The rate of etching and re-deposition could be determined from the time-to-saturation measurements of the weight change of exposed samples. Figures 2 and 3 illustrate the weight loss trend for both the S/200 and S/500 films in both plasma treatment regimes. It is obvious from the figures that surface etching immediately starts when exposing the films to the plasma. The time-to-saturation, as seen in Figures 1 and 2, indicates the threshold to a re-deposition-dominating regime. This behavior indicates competing etching and re-deposition effects in a closed geometry exposure configuration. For the helium-exposed films, the maximum weight loss is at approximately 1-min exposure, and the oxygenated-helium treated samples reached a maximum weight loss at 2 min exposure. This, in correlation with the enhanced peak magnitude of the oxygenated-helium samples, shows that the presence of oxygen in the discharge provides a higher etching rate when compared to etching in helium-only plasma. Charge exchange may also be responsible for the production of oxygen ions when the test cell is operated using only helium. Typically, helium is not considered an etchant gas, but under atmospheric conditions its etching ability is altered. This is because of the fact that the test cell will always contain a fraction of air, which includes the presence of nitrogen and oxygen. With the presence of air, charge exchange can occur between nitrogen and oxygen[13]:

$$N^+ + O \rightarrow N + O^+$$

The result of this charge exchange causes an increase in the formation of oxygen ions, which induces etching of the substrate. Etching will be increased

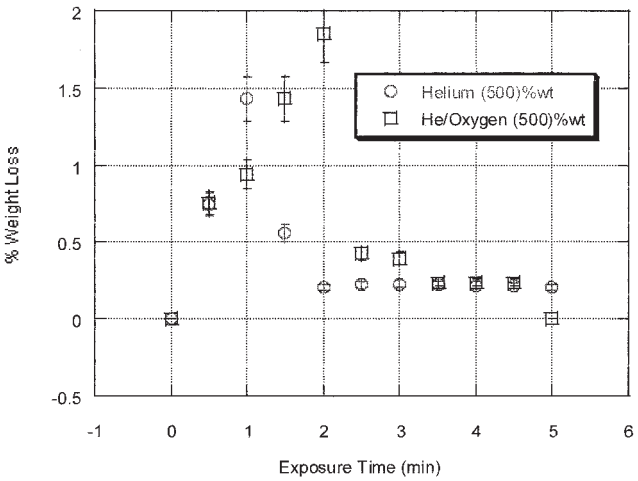

Figure 3 Percent weight loss versus exposure time for PET 500 treated in helium and oxygenated-helium plasmas.

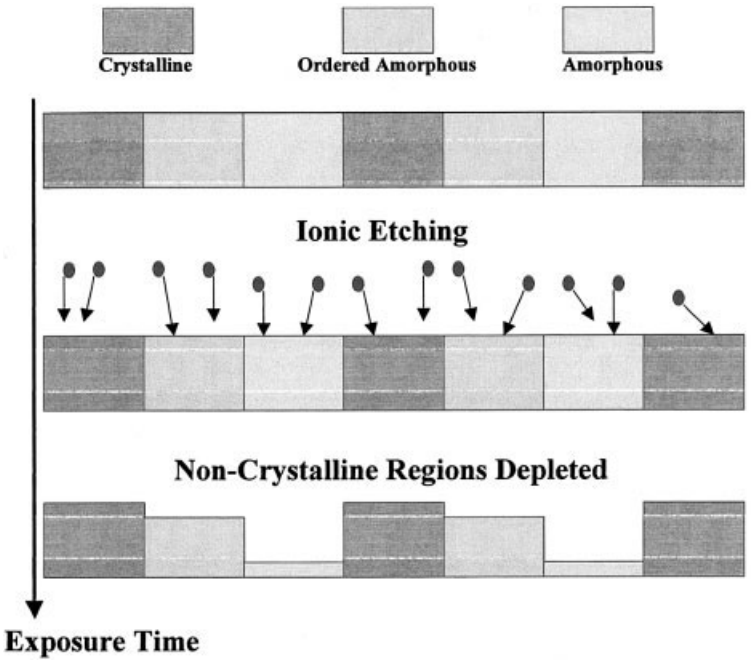

Figure 4 Schematic illustration of etching PET in atmospheric plasma treatment showing time evolution of selective etching.

further by the addition of oxygen to the feed gas forming oxygenated-helium plasma.

Model for etching mechanism

For mono-phase surfaces exposed to an ion flux from nonthermal plasma, the etching is expected to be uniform over the entire surface, with a constant etching rate. When a polyphase surface is exposed to the ion flux, the expected etching rate will be determined by the difference between the phases and their corresponding composition. Differential or selective etching of a polyphase surface depends on the particle flux and molecules leaving the surface at different rates as determined by each phase. The time-dependent relation between the degree of solubility and surface etching may be linear or nonlinear depending on the difference between these phases. The total surface etching may be expressed by the sum of all etching rates δw on the surface:

$$\delta w = \frac{\sum_j n_j}{\Phi} \quad (1)$$

where n_j is the etch rate of the specific phase and Φ_j is the number of phases in the substrate.

Relating the degree of solubility D_s to the exposure time of the film to the plasma ion flux and composition may be expressed by either a linear (eq. (2)) or a nonlinear (eq. (3)) decay function with respect to δw:

$$D_s = G - (\delta w)\tau \quad (2)$$

$$D_s = Ge^{-(\delta w)\tau} \quad (3)$$

where τ represents plasma exposure time and G is a gas determined constant.

For PET the surface is a three-phase composition,[14–16] in which 40% is crystalline and 60% is a combination of amorphous and ordered amorphous phases. Thus, for PET, eq. (1) could be re-written as:

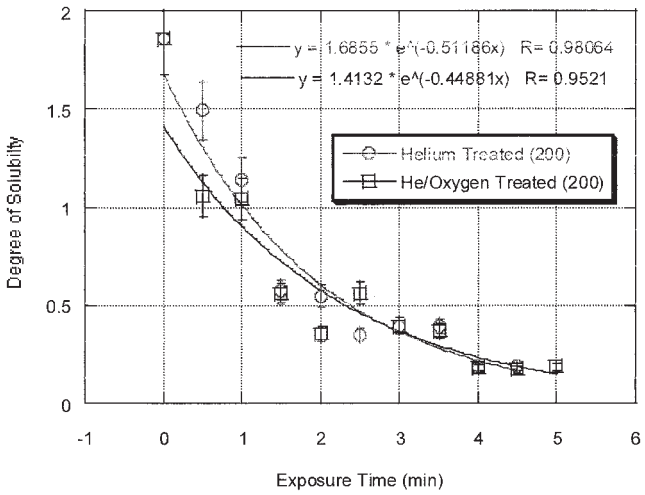

Figure 5 Degree of solubility versus exposure time for PET 200 treated in helium and oxygenated-helium plasmas, and fitted data to exponentially decaying function.

$$\delta w = \frac{n_{\text{amorphus}} + n_{\text{ordered amorphus}} + n_{\text{crystalline}}}{3} \quad (4)$$

Based on this equation and the contribution of each phase to the total surface etching, a mechanism could be explained as shown in Figure 4. Due to the high order and high bond energy in the crystalline phase, it is assumed that etching of the crystalline regions, $n_{\text{crystalline}}$, is almost zero. Etching of the crystalline phase may be induced with a stronger etchant gas species; however, this will be a small yield and $n_{\text{crystalline}}$ will still be negligible. This means that the ratio of n/Φ for PET will vary between 1/3 and 2/3.

Solubility

Because solubility is directly related to the material's ability to swell in solution, portions of each film were soaked in a swelling agent and the effects of plasma exposure on the films' solubility was determined. Since swelling occurs in the amorphous regions, a decrease in the swelling ability of the film was predicted. Plots of the percent weight change in films before and after soaking revealed that the degree of swelling decreased with increasing plasma exposure time for both species, which supports the mechanism of selective etching. As exposure time increases, etching increases, specifically in the amorphous regions, causing an increase in percent crystallinity and a decrease in solubility. The decreasing solubility trend shows the rate of change slowing after 1.5 min for helium exposed films, and after 2 min for the oxygenated-helium exposed films. This corresponds to the weight loss trend previously discussed. It should also be noted that the S/200 and S/500 measurements have an order of magnitude difference due to their difference in thickness.

Further analysis of the solubility revealed an exponentially decaying trend versus a linear trend. This is illustrated in Figures 5 and 6. Using eqs. (3) and (4), the final model can be written as:

$$D_s = Ge^{-(n/3)\tau} \quad (5)$$

Investigation of the experimental results revealed that the n/Φ ratio for all samples falls within the predicted range of 1/3 to 2/3. For the S/500 films treated in helium-only regime, the n/Φ ratio is 0.304; but once oxygen is added to the plasma, the n/Φ ratio increases to 0.366. This shows a slight increase in the etching rate for the oxygenated-helium treatment due to oxygen's strong etching ability. For the helium-only treated film n equals 0.912, and for the oxygenated-helium treated films n equals 1.099. This indicates that both films had almost 100% of the surface amorphous regions removed.

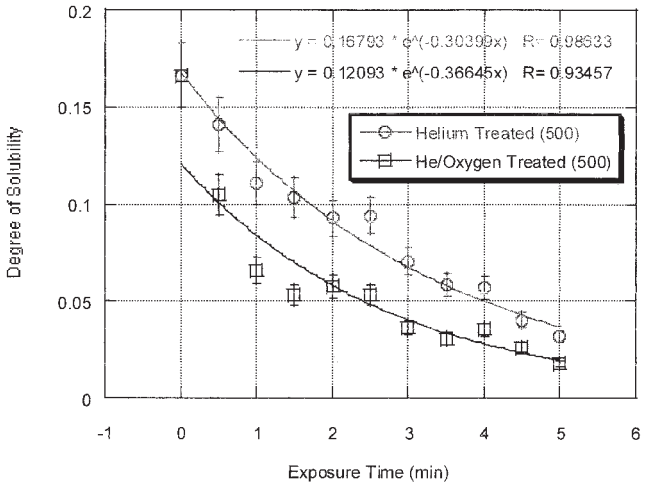

Figure 6 Degree of solubility versus exposure time for PET 500 treated in helium and oxygenated-helium plasmas, and fitted data to exponentially decaying function.

The S/200 films showed less difference between the helium treatment and the oxygenated-helium treatment. Specifically, the helium treated films had an n/Φ ratio of 0.5119 and the oxygenated-helium treated films had an n/Φ ratio of 0.4488. This relates to n values equaling 1.536 and 1.346, respectively. These values are much higher than those observed with the S/500 films, and show not only a complete etching of surface amorphous regions, but additional etching of the ordered amorphous regions as well. These differences are most likely due to the difference in the film thickness. Since the S/200 films are thinner, they will therefore show a more notable etching effect. This correlates directly to the weight loss trend. Surface roughening shown through AFM analysis[17] also confirms this theory.

CONCLUSION

Several effects were observed when exposing PET films to atmospherically generated helium and oxygenated-helium plasmas. Weight loss steadily increases with increased exposure time due to etching effects. This continues until saturation, which then shifts the trend to re-deposition of previously etched film material. Percent crystallinity increases as a result of selective amorphous etching. The developed model, which relates degree of solubility to the total rate of etching and number of phases on the surface, correlates well with the experimental results. The degree of solubility decreases following an exponential decay law, which is directly affected by the substrate and plasma composition.

Future work

Future work in this area will include experiments in an open geometry to compare to the results obtained

in this closed geometry work. Tests will also include the use of fluorocarbon gases to assess their high etching effect and to determine the gas-dependent parameter in the developed model.

The authors gratefully acknowledge the assistance of Brian Bures during the course of this research, and his help in providing an insight on device operation and experimental procedure.

References

1. Simionescu, C. I.; Denez, P.; Macoveanu, M. M.; Negulescu, I. Makromol Chem Suppl 1984, 8, 17.
2. Nakayama, Y.; Soeda, F.; Ishitani, A.; Ikegami, T. Polymer Engineering and Science 1991, 31, 812.
3. Placinta, G.; Arefi-Khonsari, F.; Gheorghiu, M.; Amouroux, J.; Popa, G. J Appl Polym Sci 1997, 66, 1367.
4. Gupta, B.; Hilborn, J.; Hollenstein, C. H.; Plummer, C. J. G.; Houriet, R.; Xanthopoulos, N. J Appl Polym Sci 2000, 78, 1083.
5. Padhye, M. R.; Bhat, N. V.; Mittal, P. K. Textile Research J 1996, 66, 502.
6. Laishun, S. European Polymer J 2000, 36, 987.
7. Park, S.-C.; Koh, S.-K.; Pae, K. D. Polymer Engineering and Science 1998, 38, 1185.
8. Wakida, T.; Kawamura, H.; Song, J. C.; Goto, T.; Takagishi, T. Sen-I Gakkaishi 1986, 73, 384.
9. Shi, L. J of Polymer Engineering 1999, 19, 445.
10. Wakida, T.; Tokino, S.; Niu, S.; Kawamura, H. Textile Research J 1993, 63, 433.
11. Gray, A. P. Thermocemica Acta, 1970, 1, 563.
12. Okuno, T.; Yasuda, T.; Yasuda, H. Textile Research J 1992, 62, 474.
13. Lieberman, M. A.; Lichtenber, A. J. Principles of Plasma Discharges and Materials Processing; John Wiley & Sons, Inc.: New York, 1994.
14. Cole, K. C.; Ajji, A.; Pellerin, E. Macromolecules 2002, 35, 770.
15. Prevorsek, D. C. J Polym Sci, C 1971, 32, 343.
16. Prevorsek, D. C.; Tirpak, G. A.; Harget, P. J.; Reimschuessel, A. C. J Macromol Sci –Phys B 1974, 9, 733.
17. Hwang, Y.; Matthews, S. R.; McCord, M. G.; Bourham, M. A. J Electrochem Soc 2004, 151, C495–C501.